



HAL
open science

GABAergic transmission underlies interictal epileptogenicity in pediatric FCD

Thomas Blauwblomme, Elena Dossi, Christophe Pellegrino, Emmanuelle Goubert, Beatriz Gal Iglesias, Christian Sainte-Rose, Nathalie Rouach, Rima Nabbout, Gilles Huberfeld

► **To cite this version:**

Thomas Blauwblomme, Elena Dossi, Christophe Pellegrino, Emmanuelle Goubert, Beatriz Gal Iglesias, et al.. GABAergic transmission underlies interictal epileptogenicity in pediatric FCD. *Annals of Neurology*, 2018, 10.1002/ana.25403 . hal-01971710

HAL Id: hal-01971710

<https://amu.hal.science/hal-01971710v1>

Submitted on 7 Jan 2019

HAL is a multi-disciplinary open access archive for the deposit and dissemination of scientific research documents, whether they are published or not. The documents may come from teaching and research institutions in France or abroad, or from public or private research centers.

L'archive ouverte pluridisciplinaire **HAL**, est destinée au dépôt et à la diffusion de documents scientifiques de niveau recherche, publiés ou non, émanant des établissements d'enseignement et de recherche français ou étrangers, des laboratoires publics ou privés.



GABAergic transmission underlies interictal epileptogenicity in pediatric FCD

Thomas Blauwblomme^{1,2,3}, Elena Dossi⁴⁺, Christophe Pellegrino⁵⁺, Emmanuelle Goubert⁵⁺, Beatriz Gal Iglesias⁶, Christian Sainte-Rose^{1,2}, Nathalie Rouach⁴, Rima Nababout^{2,7}, Gilles Huberfeld^{3,4,8}.

1. APHP, Department of Pediatric Neurosurgery, Hospital Necker, Paris, France
2. Université René Descartes. PRES Sorbonne Paris Cité, Paris, France
3. INSERM U1129, Infantile Epilepsies and Brain Plasticity, Paris Descartes University, PRES Sorbonne Paris Cité, Paris, France
4. Neuroglial Interactions in Cerebral Physiopathology, Center for Interdisciplinary Research in Biology, Collège de France, CNR UMR 7241, INSERM U1050, Labex Memolife, PSL Research University, Paris, France
5. INMED, INSERM 1249, Aix-Marseille Univ, Marseille, France
6. Facultad de Ciencias Biomédicas y de la Salud, Universidad Europea, Madrid, Spain
7. APHP, Department of Neuropediatrics, Hospital Necker, Paris, France
8. Sorbonne University, AP-HP, Department of Neurophysiology, La Pitié-Salpêtrière Hospital, Paris, France

⁺ These authors contributed equally

Running title:

GABAergic interictal epileptic mechanisms in FCD

Corresponding author:

Thomas Blauwblomme
Service de Neurochirurgie Pédiatrique, Hôpital Necker
149 rue de Sevres, 75015 Paris, France
Mail: thomas.blauwblomme@aphp.fr
Tel: +33144494252
Fax: +33144494243

Key Words:

Focal Cortical Dysplasia, Malformations of cortical development, In vitro recordings, NKCC1, KCC2, Cation chloride co-transporter, GABA, Epilepsy Surgery

Abbreviations:

CB-PV+: calbindin parvalbumin; FCD: Focal Cortical Dysplasia; HFO: High Frequency oscillations; IID: Interictal Discharges; KCC2: Potassium-Chloride-co-transporter 2; LVFA: low voltage fast activity; NKCC1: Sodium-Potassium-Chloride-co-transporter 1PID: Preictal Discharges; SEEG: stereo electro encephalography.

This article has been accepted for publication and undergone full peer review but has not been through the copyediting, typesetting, pagination and proofreading process, which may lead to differences between this version and the Version of Record. Please cite this article as doi: 10.1002/ana.25403

ABSTRACT

Objective: Dysregulation of GABAergic transmission has been reported in lesional acquired epilepsies (gliomas, hippocampal sclerosis). We investigated its involvement in a developmental disorder, human Focal Cortical Dysplasia, focusing on chloride regulation driving GABAergic signals.

Methods: *In vitro* recordings of 47 human cortical acute slices from 11 pediatric patients operated from a Focal Cortical Dysplasia were performed on Multi Electrode Arrays. GABAergic receptors and chloride regulators were pharmacologically modulated. Immunostaining for chloride co-transporter KCC2 and interneurons were performed on recorded slices to correlate electrophysiology and expression patterns.

Results: Focal Cortical Dysplasia slices retain intrinsic epileptogenicity. 36/47 slices displayed spontaneous interictal discharges, along with a pattern specific to the histological subtypes. Ictal discharges were induced in pro-epileptic conditions in 6/8 slices in the areas generating spontaneous interictal discharges, with a transition to seizure involving the emergence of preictal discharges. Interictal discharges were sustained by GABAergic signaling as a GABA_A receptors blocker stopped them in 2/3 slices. Blockade of NKCC1 Cl⁻ co-transporters further controlled interictal discharges in 9/12 cases, revealing a Cl⁻ dysregulation affecting actions of GABA. Immunohistochemistry highlighted decreased expression and changes in KCC2 sub-cellular localization and a decrease in the number of GAD67-positive interneurons in regions generating interictal discharges.

Interpretation: Altered chloride cotransporters expression and changes in interneuron density in FCD may lead to paradoxical depolarization of pyramidal cells. Spontaneous interictal discharges are consequently mediated by GABAergic signals and targeting chloride regulation in neurons may be considered for the development of new antiepileptic drugs.

INTRODUCTION

Malformations of cortical development are an emblematic etiology of drug resistant lesional epilepsy in children. Since the pioneer description of focal cortical dysplasia (FCD) by Taylor¹, the classification has evolved in 3 main types of FCD according to the pattern of dyslamination, the presence of abnormal cells (cytomegalic neurons and balloon cells), and the association with another brain lesion^{2,3}. This histological classification is crucial to categorize the various features of FCDs but it does not describe the mechanisms of the genesis of epileptic activities, nor does it incriminate a subtype of abnormal cell, neuronal network or a causal molecular defect. Moreover, the onset site of the epileptic discharges remains to be assessed within the histological defect or at its boundary with the surrounding cortex. This is a key issue since surgical resection, that is often the main therapeutic option, fails to cure about 40% of patients, mainly in type I FCD, presumably because of incomplete resection or because distant areas display high epileptogenicity in a complex epileptic network⁴⁻⁶. Mapping epileptic activities in various types of FCDs is therefore mandatory to optimize the extent of their resection. Postsurgical FCDs tissues thus offer a unique opportunity to study epileptogenicity mechanisms that should pave the way for new targeted therapies.

Enhanced excitatory neurotransmission has been shown in dissociated neurons from human FCD. Increased NMDA currents, reduced Mg^{2+} sensitivity along with a decreased expression of the NR2B subunit⁷, as well as abnormal features of GABAergic neurotransmission have also been involved in FCD's epileptogenicity. The number of inhibitory interneurons is globally reduced in type I-III FCD, while rearrangement of their cortical distribution is seen in type II FCD⁸⁻¹⁰. In the focal neonatal cortex freeze-lesion animal model of dysplasia, interneurons accumulate at the boundary of the lesion and ambient GABA is increased¹¹. Moreover, in cortical slices from human postoperative FCD tissues, ictal-like events which are pharmacologically induced *in vitro*, are abolished by hyperpolarizing interneurons or blocking GABAergic transmission¹². In dissociated neurons from human FCDs, GABAergic currents of cytomegalic neurons exhibit immature features consisting in modified sensitivity to zolpidem and zinc and prolonged opening time¹³ and display a pacemaker $GABA_A$ receptor-mediated activity¹⁴. However, as in other human epileptic conditions such as hippocampal sclerosis¹⁵ or gliomas¹⁶, the shift to excitatory effects of GABAergic signals may contribute to FCD epileptogenicity. Previous studies have reported chloride co-transporters (Sodium-Potassium-Chloride-co-transporter 1 (NKCC1) and Potassium-Chloride-co-transporter 2 (KCC2)) expression abnormalities in both neonatal cortex freeze-lesion animal model of FCD and in human FCD¹⁷⁻¹⁹. This may result in increased neuronal chloride concentration and a shift towards depolarizing responses to GABA²⁰. Other studies also showed that ictal discharges are initiated by interneurons and controlled by $GABA_A$ receptor blockade. However, these studies were not systematically performed at the network level and a precise mapping of epileptic activities within the malformations themselves was not performed to seek for local variability. They were specifically limited by the absence of spontaneous interictal discharges (IIDs) which, in our work, allowed assessment of epileptic areas.

We here report that spontaneous IIDs can be recorded *in vitro* from acute cortical slices of human postoperative FCD. GABAergic signals positively participated to their genesis since IIDs were blocked by $GABA_A$ receptors antagonists. This effect was related to perturbations of neuronal chloride regulation with a modification of KCC2 expression and an excess of activity of its counterpart NKCC1. Indeed, NKCC1 blockade by bumetanide controlled epileptic discharges.

METHODS

Patient's parents or legal guardians gave informed written consent according to the Internal Review Board protocol (n° D2009-955 for storage of brain samples).

Patients selection and surgery

Cortical samples were obtained from 11 children with focal epilepsies and FCDs operated for drug resistant epilepsy during a two-year period. 7 other patients with FCD were not included in this study as their cortex was not recorded in vitro, either because the parents refused to be enrolled in the study, or because of technical issues in the operating room or organizational mismatch between clinical and research teams.

Surgery was planned after multimodal preoperative evaluation including video-EEG recording, neuropsychological examination, MRI and ¹⁸FDG PET scan. When required, intracranial chronic recording was performed according to the SEEG methodology. Antiepileptic drugs were maintained during the perioperative course. General anesthesia was induced with intravenous propofol injection and maintained by inhaled sevoflurane and intravenous sufentanyl. Surgery was not modified for the research protocol and consisted in lobar or gyral "en bloc" resection, performed via a subpial technique, avoiding excessive specimen manipulation or coagulation, as intraoperative crush injury can cause loss of NeuN and other neuronal immunoreactivities²¹.

Specimens were taken in the presumed ictal onset zone, defined either by SEEG, or EEG and imaging (Fig. 1) and histological diagnosis was assessed according to the ILAE recommendations²².

A total of 11 pediatric patients were included in the study. Clinical data are summarized in the table. Briefly, M/F ratio was 1.2, mean duration of epilepsy was 4.5 years (range: 0.7-13.9 y; SD: 4.2), age at surgery was 8 years old (range: 0.9-16.9 y; SD: 4.6), localization of the epileptogenic zone was frontal (n=4), temporal (n=4), or in the posterior quadrant (n=3).

Histology was FCD type I (Ib n=1, Ic n=4), FCD type IIb (n=3) and FCD type III (IIIA n=2, IIIB n=1).

Tissue Preparation

Cortical specimen were immediately placed in the operative room in iced sucrose-based ACSF containing (in mM): 250 sucrose, 3 KCl, 25 NaHCO₃, 10 D-Glucose, 1 CaCl₂, 10 MgCl₂, equilibrated with 5% CO₂ in 95% O₂, and transported to the laboratory^{15,23,24}. Meninges, blood clots and vessels were gently removed and 400 µm neocortical transverse slices were cut with a vibratome (HM650V, Microm Microtech, France). Slice were stored in an interface chamber (Brain Slice Chamber 2, Scientific Systems Design, USA) at 37°C and continuously perfused with ACSF containing (in mM): 124 NaCl, 3 KCl, 26 NaHCO₃, 10 D-Glucose, 1.6 CaCl₂, 1.3 MgCl₂, oxygenated with carbogen (5% CO₂ in 95% O₂), at 2 ml/min during at least 1 hour.

MEA recordings

A total of 47 slices were studied. 29 cortical slices were placed on planar micro electrode arrays petri dishes (Multi Channel Systems, Germany) organized in 12x10 layout grids, with an electrode diameter of 30 µm, and an inter-electrode interval of 1500 µm / 1000 µm. 18 cortical slices were recorded on a smaller MEA organized in a 12x12 matrix with an electrode diameter of 30 µm and an inter-electrode interval of 200 µm (Multi Channel Systems, Germany). Cortical slices were kept in place by using a platinum anchor and continuously perfused with ACSF at a rate of 6 ml/min at 37°C. Pictures of cortical slices on

MEAs were acquired with a video microscope table (MEA-VMT1; Multichannel Systems, Germany) through MEA Monitor software (Multichannel Systems, Germany) to identify the location of the electrodes relative to the pial surface of the slices. Electrophysiological activities were recorded with the MEA 2100-120 system (bandwidth 1-3000 Hz, gain 5x, Multichannel Systems, Germany) through MC_Rack 4.5.1 software (Multichannel Systems, Germany) and sampled at 10 kHz. The spontaneous activity of the slices was recorded in physiological ACSF containing (in mM) 124 NaCl, 3 KCl, 26 NaHCO₃, 1.6 CaCl₂, 1.3 MgCl₂ and 10 D-glucose.

Pharmacological studies for IIDs were performed in modified physiological ACSF containing Bumetanide (8 μM) or Picrotoxin (100 μM). Ictal-like activity was induced by perfusing the slices with high potassium (6-8 mM), magnesium free pro-epileptic ACSF (0 Mg²⁺ - 6-8 K⁺ ACSF) as described in vitro in rodent's tissues. In humans, such low Mg²⁺ / high K⁺ 'proconvulsant' solution triggers seizure-like events in vitro only in the cortex from epileptic patient in which spontaneous interictal discharges are recorded³¹.

We included in this study only the slices generating spontaneous IIDs.

All the recordings were performed in dysplastic cortex; in FCD III, we did not include peri-tumoral cortex (ganglioglioma) or hippocampal sclerosis that were located on the mesial part of the temporal lobe.

Histology.

After MEA recordings, slices were fixed in 4% Zn Formalin (Microm, Microtech, France) for 24 hours. After intense PBS 1X wash, sections were permeabilized and blocked in PBS with 0.3 % Triton X-100 and 5 % normal goat serum (NGS) for 1 h at room temperature. Incubation with primary antibodies diluted in PBS with 5 % NGS and 0.1 % Triton X-100 was carried out at 4°C overnight using anti-NeuN (Millipore, Bachem, 1:1000), anti-pan-KCC2 (homemade, Ludwig et al., 2003²⁵) and anti-GAD67 (Millipore, MAB5406). After rinsing 3 times in PBS, slices were incubated with the corresponding Alexa Fluor-conjugated secondary antibodies diluted in PBS (1/500, Invitrogen) for 2 h at room temperature and finally counterstained for 1 min with Hoechst 33258 (10 μg/ml in PBS, Sigma-Aldrich). Sections were then mounted onto Superfrost Plus glass slides in Fluoromount G mounting medium. For each section, images were taken using a confocal microscope with 10x, 20x or 40x objectives. Expression of KCC2 and GAD67-PV (Parvalbumin) was compared between zones generating IIDs and silent zones, as defined by in vitro MEA recordings. KCC2 expression was analyzed using single cell analysis under the Plot Profil Plugin in ImageJ, as described in Tyzio et al, 2014, by plotting fluorescence intensity along the cell and comparing epileptic areas to silent areas identified by MEA recordings²⁶. Delimitation of epileptic and non-epileptic areas was done considering all layers of a square of 2000 μm, corresponding to the area surrounding a MEA electrode.

Morphological analysis was performed after slicing the remaining tissue, and immunostaining with Nissl and NeuN. We did not study the white matter.

ILAE criteria were used for the classification of FCDs as follows: FCD I refers to radial (Ia), tangential (Ib) or mixed (Ic) dyslamination of the neocortex, FCD II are characterized by dysmorphic neurons without (IIa) or with balloon cells (IIb), FCD III is defined by the association of dyslamination to a lesion³.

Electrophysiological Analysis and Statistics

Local Field Potentials (LFPs) were analyzed with Clampfit software (pClamp Software, Molecular Devices), using visual analysis and the automated event detector toolbox via threshold detection. Statistical analysis was performed on IBM SPSS Statistics software. Results were expressed as mean +/- standard deviation, and significance level was set at

$p < 0.05$. Intergroup analysis was done with non-parametric Kruskal Wallis test, and Wilcoxon test for repeated measurement on a single sample.

Visual analysis of the LFP matrix under MC-Data software (Multichannel Systems, Germany) was used to count the number of contacts displaying consistent IIDs. The area of cortex generating IIDs was then calculated by multiplying with the surface underneath each electrode (product of horizontal (1500 μm) and vertical (1000 μm) inter electrode distance = 1.5 mm^2). The depth of IID initiation was measured orthogonally to the tangent of the pial surface between the pia and the electrode contact showing either phase inversion or maximum amplitude.

High frequency oscillations (HFOs) were analyzed with Ripple Lab[®], according to previously described methodology²⁷. Briefly, after filtering (80-500 Hz), and time-frequency analysis with the wavelet transform, HFOs were either visually detected, or automatically detected using Hilbert method. Duration and mean frequency of the HFO events were then noted for IIDs and pre-ictal discharges (PIDs), respectively.

Seizures were analyzed with Spike 2 software using time frequency representation and classified according to the discharge frequency and pattern as oscillatory (<20Hz) or low voltage fast activity (LVFA) event.

RESULTS

Postoperative tissues from human FCD retain intrinsic epileptic activities in vitro

FCD slices generate spontaneous IIDs

47 slices from 11 patients were studied on MEAs (median: 4 slices/patient). Spontaneous IIDs were recorded in 36 slices (76.5 %) in physiological ACSF (Fig. 2A). IIDs were generated at a mean depth of 2 mm (\pm 1 mm) from the pial surface, and the mean cortical surface displaying IIDs was 7.4 mm² (\pm 2.9), corresponding to 8.9 % of the cortical surface explored with MEA contacts (on the large 12x10 matrix). We observed a rhythmic pattern of IIDs, with a mean frequency of 1.59 Hz (\pm 1.03, n = 3678 events from 36 slices), a mean duration of 67.9 ms (\pm 70.8 ms), and a mean amplitude of 23.8 μ V (\pm 14.2).

IID pattern varied according to the FCD histological type (Fig. 2B,C). Types I and II FCDs produced IIDs with variable amplitude and duration while type III FCDs generated homogeneous, regular IIDs. The electrode surface recording IIDs was smaller (Mann-Whitney test, $p < 0.001$, 28 slices) in FCD III (4.8 mm² \pm 1.2) than in FCD type I (9.2 mm² \pm 2.8) or FCD type II (7.3 mm² \pm 2.7). IID occurrence was more frequent both in FCD IIb (1.72 Hz \pm 0.8, n = 543 events from 10 slices, Kruskal Wallis test, $p < 0.001$) and FCD I (1.71 Hz \pm 1.1) than in FCD III (1.24 Hz \pm 0.7), with a shorter duration of IIDs in type II (52.47 ms \pm 46.1, Kruskal Wallis test, $p < 0.001$) than in type I (63.5 ms \pm 58.3, n = 1914 events from 17 slices) or III (79.4 ms \pm 92.1, n = 1221 events from 9 slices; Fig. 2C). IID amplitude, known to vary from one slice to another, was smaller in FCD III (19.2 μ V \pm 15.5, n = 1221 events, Kruskal Wallis test, $p < 0.001$) than in FCD I (25.9 μ V \pm 13.1) and II (26.8 μ V \pm 12.5).

When comparing patients < 5 years old (yo) to patients > 5 years old, age was found to have a statistically significant effect on IID patterns (Mann Whitney test, $p < 0.01$). Indeed, IID occurrence was more frequent after 5 yo (1.8 \pm 1 Hz) than before 5 yo (0.2 \pm 0.4 Hz) with a larger amplitude at > 5 yo (27.1 μ V \pm 12) than < 5 yo (13.9 μ V \pm 9.2) and a shorter duration (55.5 ms \pm 48.2) after 5 yo than before (125.2 ms \pm 88).

FCD slices generate seizure-like events in pro-epileptic conditions

Pro-ictogenic conditions (0 Mg²⁺ - 6-8K⁺ ACSF)²⁸ elicited ictal-like discharges in 6/8 slices from 5 different patients (FCD Ic n=2, FCD III n=3) (Fig. 3A). FCD type II were not studied in pro-epileptic conditions. The first seizure occurred after a mean delay of 1057 s (range: 255-2695, SD: 901, n = 6 slices), and was preceded by large amplitude PIDs in 5/6 cases, as already described in human tissues such as the subiculum in cases of hippocampal sclerosis²⁵ or peritumoral neocortex¹⁶.

Seizures then recurred with a mean interval of 84 s (range 11.7-342, SD: 84.3). Mean seizure duration was 73.3 s (range: 25.3-206.3, SD: 38.4) and was not statistically different between the 3 histological subtypes (Kruskall Wallis test, $p = 0.583$). Among the 40 seizures recorded, the discharge pattern was a low voltage fast activity (LVFA) with a mean frequency of 134.4 Hz (range: 119-148, SD: 10.8) followed by rhythmic bursts in 15 cases, and an oscillatory pattern with direct rhythmic bursts (synchronous pattern) occurring at a frequency of 10.6 Hz (range: 2.7-25, SD: 8.4) in the remaining cases (n = 25; Fig. 3B). The discharges pattern was stable over time as in 84 % of the slices, the first recorded seizure was followed by an identical type of discharge, regardless of the histological subtype. However, the seizure pattern evolved during the course of the recording in 3/6 slices displaying ictal discharges, the inaugural seizure representing the majority of the seizure patterns subtype during the recording in 3/6 cases. The seizure onset pattern was significantly different between FCD type

I and FCD type III (chi square test, $p=0.008$), as sharp activity was noted in 9/9 seizures in FCD type I, as compared to 16/31 in type III.

In most cases, the area generating IIDs overlapped regions generating ictal-like events (Fig. 3A) and the surface of the cortex displaying seizure activity increased as compared to IIDs on the large MEA (4 slices), from 6 mm^2 (± 3.2) to 15 mm^2 (± 7.8). However, in one case (FCD III), ictal discharges emerged simultaneously in 2 distinct areas with the same electrophysiological pattern (distant from 4 mm); interestingly, one of the two areas had no previous IIDs.

The transition to seizure is progressive and characterized by the emergence of PreIctal Discharges (PIDs)

During the transition from the basal interictal state to pharmacologically-induced seizures, transient events with larger field potentials emerged, and could be distinguished from IIDs, as they displayed an amplitude increasing as a function of time (Pearson correlation = 0.556, $p<0.001$; Fig. 3A). PIDs ($n = 373$ from 5 slices) appeared 293.9 s (range 9.8-648, SD: 244) before seizures, and their amplitude and duration ($51.9 \mu\text{V}$, range 12.5-162 μV , SD: 33.8; 69.8 ms, range 5.4-399 ms, SD: 49) were significantly larger (Mann-Whitney test, $p<0.001$) than coexisting IIDs ($11.5 \mu\text{V}$, range: 4-29 μV , SD: 4; 24.4 ms, range: 5.4-174 ms, SD: 136). IID frequency was significantly higher (Mann-Whitney test, $p<0.001$) than PID's ($0.89 \text{ Hz } \pm 0.74$ vs $0.48 \text{ Hz } \pm 0.34$ for IIDs and PIDs, respectively).

In the rhythmic bursts seizure pattern ($n = 15$ seizures), clear PIDs preceded seizure onset in 12/25 cases, but were lacking in the other 13/25 ones. In LVFA seizures ($n = 15$) PIDs preceded the fast tonic discharge at seizure onset in 13/15 cases, whereas LVFA occurred in 2/15 cases without preceding PIDs. PIDs were therefore significantly associated with the LVFA pattern (chi square test, $p=0.014$). PIDs were not significantly associated with histological subtypes (chi square test, $p=0.2$), as they were noted in 4/9 and 21/31 seizures in FCD type I and III respectively. PID amplitude was not different according to histology (Mann Whitney test, $p=0.265$), but their frequency was higher (Mann Whitney test, $p=0.002$) in FCD type I (mean: 0.49 Hz) than in FCD type III (mean 0.18 Hz) Moreover, PIDs displayed HFOs (mean: 271.63 Hz, SD: 73.1, $n = 61$ events from 4 slices) during the first half of the spike (mean duration: 42.28 ms, SD: 14.5), whereas IIDs displayed only multi-unit activity without an oscillatory pattern (Fig. 3B). HFO frequency was not different according to histological subtype (Mann Whitney test, $p= 0.111$).

Epileptic activities correlate to histological defects

Histological analysis was done after MEA recording in 5 slices with sufficient specimen quality and quantity (FCD IIb, $n = 2$; FCD Ic, $n = 1$; FCD IIIa, $n = 2$). It confirmed that the areas generating IIDs were within the FCD and presented dyslamination (4 cases) (Fig. 1D) or dysmorphic neurons (1 case). However, there was no obvious heterogeneity in terms of cellular or architectural abnormalities in slices, for instance when comparing areas generating IID to silent zones.

Epileptic interictal discharges are associated with altered GABAergic inhibition

GABAergic neurotransmission is involved in IID generation

To test whether GABAergic signaling is positively involved in the production of epileptic activities in human dysplastic tissues¹², we studied GABA_A signaling in 3 slices from 3 patients (FCD type Ic, IIb, and IIIa) by applying the specific antagonist picrotoxin (100 μM). In 2 out of the 3 slices, picrotoxin stopped IIDs after a delay of 90 and 1001 seconds respectively (Fig. 4A). In the third slice (FCD type Ic), IID frequency in picrotoxin

(0.5 Hz \pm 0.27) was significantly (Mann Whitney test, $p < 0.001$) lower than in physiological ACSF (0.9 \pm 0.7 Hz).

To investigate an alteration in inhibitory networks¹⁰, we quantified the total number of interneurons within the cortical areas in 3 slices producing IIDs (FCD_{Ic} n = 2, FCD IIIa n = 1) compared to zones devoid of epileptic activity in 4 slices. We compared the number of GAD67 cells in epileptic area to non-epileptic areas, as detected by MEA recordings, considering all layers of a column of 2000 μ m, corresponding to the area surrounding a MEA electrode (Fig. 4B). In epileptogenic areas, the total number of GAD67-positive cells (normalized mean: 0.53 \pm 0.19) was significantly reduced (Mann-Whitney test, $p = 0.0018$) compared to the areas in which no epileptic discharge was recorded (normalized mean: 0.95 \pm 0.43).

Chloride co-transporters abnormalities support epileptic activities genesis.

Low neuronal chloride concentration is maintained in mature neurons mainly by the expression of the Cl⁻ extruder KCC2, together with the repression of the Cl⁻ loader NKCC1²⁹. We explored the activity of NKCC1 and the expression of KCC2 in dysplastic tissues with perturbed GABAergic signaling.

The effects of the specific blockade of the chloride co-transporter NKCC1 by the diuretic bumetanide was assessed in 12 slices from 7 patients. Bumetanide (8 μ M) suppressed IIDs in 9/12 slices with a mean delay of 1205 s (\pm 670) (Fig. 5A). IIDs reappeared after washout in physiological ACSF with a mean delay of 422 s (\pm 290). In the remaining 3 cases, bumetanide had no effect in one case of FCD type Ic and was associated with a reduction of both frequency (2.06 \pm 0.8 vs 1.5 \pm 0.8 Hz) and amplitude (21.8 \pm 5.9 vs 20.1 \pm 4.8 μ V) in two cases of FCD type Ic (Mann-Whitney test $p < 0.001$). These data show that presumed up-regulated NKCC1 contributes to the production of IIDs. However, due to the lack of specific antibody, we were not able to study its expression by immunocytochemistry.

Considering both the intrinsic activity and the effect of bumetanide on slices, we then investigated the expression and the subcellular localization of KCC2 using single cell analysis by plotting fluorescence intensity along the cell and comparing epileptic areas to silent areas identified by MEA recordings (Fig. 5B).

The analysis done after Gaussian fitting of the curve reveals a change in the fluorescence repartition with a significant decrease of the membrane staining as confirmed by the quantitative analysis of the area under the curve (epileptic area: 181.6 vs. non-epileptic: 152.1; Kolmogorov-Smirnov test, $p < 0.001$) supporting internalization and/or altered membrane trafficking of KCC2 (Fig. 5C). These results were correlated with a quantitative analysis of the KCC2 immunoreactivity. To do so, we focused on the number of neurons exhibiting an increased cytoplasmic fraction of KCC2. We quantified KCC2 staining in silent zones versus epileptic ones and we observed a striking reduction of cells with KCC2 localized close to the membrane (65.8 % \pm 1.4 versus 10.46% \pm 1.6, $p < 0.0001$), together with an increase of the KCC2 fraction expressed in the cytoplasm (34.15 % \pm 1.4 versus 89.53 % \pm 1.6, $p < 0.0001$).

Altogether, these immunostaining results show that KCC2 is internalized and thus less able to maintain low interneuronal chloride concentration, which is mandatory for it to exert its hyperpolarizing inhibitory effects. Together with the excess of functionality of NKCC1, we suggest that it leads to increased neuronal concentration of GABA and its depolarizing, eventually excitatory effects that is responsible for epileptic activities. This assumption is ascertained by the blocking effect of GABA_A antagonists on epileptic activities.

DISCUSSION

In this study we show that slices from postoperative human pediatric dysplastic cortex retain epileptogenic properties at the network level, since they still generate spontaneous interictal epileptic discharges *in vitro*, in all three main types of dysplastic subtypes. We also observed that the electrophysiological pattern of IIDs depends on the subtype of FCD, although IIDs are spatially restricted to a portion of the slice in all FCD subtypes. We show that GABAergic signaling is actively involved in IID genesis. Putative depolarizing effects of GABA, released by interneurons which are decreased in number, is suggested to be related to a dysregulation of neuronal chloride with an excessive load by the co-transporter NKCC1 and a defective extrusion by its counterpart KCC2. We finally show that in pro-epileptic conditions, dysplastic tissues are able to generate ictal-like discharges, triggered by specific PIDs, with a high frequency oscillation signature.

This study admits several limitations. The size of our cohort is small and based on variable FCD subtypes. Thus, larger studies are needed to confirm our findings. However, work on human FCD samples is limited by the number of surgical cases and collaborative studies are difficult as these studies need to be performed on acute slices. MEA recordings were performed at the LFP level, and in acute slices, the distance between contacts and signal / noise ratio did not allow spike sorting, and therefore to attempt to categorize the neuronal subgroups initiating IIDs. Moreover, no intracellular recordings allowed identifying the cellular subtypes involvement in population discharges nor measurement of chloride-related GABAergic currents' reversal potential. Slicing the cortex has been demonstrated to alter the extracellular matrix, and to modify the chloride reversal potential³⁰, at least in superficial layers. However, in our past studies, spontaneous epileptic activities have never been recorded *in vitro* from control human tissue^{16,28,31}. Furthermore, IIDs were found to be focal and generated at a similar site in consecutive slices from the same tissue, indicating that local preexisting modifications are involved in the response rather than direct traumatism related to the slicing procedure. The morphological histological analysis was performed on 8% of the samples, and therefore these results need to be carefully interpreted.

This study brings further evidence on the epileptogenicity mechanisms of FCD. Previous studies reported several possible mechanisms underlying the epileptogenicity in FCD. Glutamatergic transmission supports ictogenesis in human FCD slices³², thanks to an increased expression and altered composition of NMDA (NR2B subunit) receptors^{7,33-35}. Alteration of the extracellular matrix through increased expression of metalloproteinase 9 leading to putative modified intra and extracellular chloride levels has been reported³⁶. Involvement of purinergic transmission was also proposed, via an excess of ATP release through pannexin 1 channels³⁷, although this pathway is not specific to FCD epileptogenesis³¹. Here, we focused specifically on GABAergic mechanisms.

First, we show that FCDs display different IID patterns according to their histology. IID frequency was higher in types I-II than in types III, suggesting that the severity of cortical disorganization was correlated with the ability to generate IIDs. These electrophysiological findings differ from previous histological studies which segregated FCD type I-III from FCD type II¹⁰. In previous studies, immunostaining of parvalbumin (PV) interneurons showed a global reduction of PV immunoreactivity in type I and III FCDs, which was not significantly different from cryptogenic cases. In type II FCDs, the number of PV/GAD65/67 neurons did not appear to be modified, but their location was redistributed¹⁰, although other studies found a clear decrease in PV interneurons, especially in layer IV in FCD IIb cases³⁸, and a global

reduction in Ila and I Ib cases³⁹. Calretinin interneurons density is itself reduced in types I and II FCDs^{39,40}. Our data point to a global reduction of interneurons, but the amount of tissues we could study did not allow correlating these alterations with FCD subtypes. Correlation between clinical, imaging, electrocorticography, histology and electrophysiological responses from dissociated neurons further suggested that in the most severe areas of FCD, glutamatergic activity is decreased, while GABAergic activity appears to be reinforced⁴¹.

Second, GABA_A receptor blockade suppressed IIDs in 2/3 cases, with limited effect in a type Ib FCD. Dysfunction of GABAergic transmission has already been demonstrated in acute human slices of FCD and on dissociated neurons. However, previous data have proposed that reduced inhibition contributed to FCD epileptogenicity or did not directly study the characteristics of GABAergic signaling in basal conditions. Whole-cell patch-clamp recordings from pyramidal cells in human FCD slices revealed reduced IPSC frequency, along with a decrease in GABA reuptake function⁸. Increased GABAergic currents were recorded in cytomegalic neurons along with a decreased sensitivity to zolpidem and zinc, thus indicating altered $\alpha 1$ and $\gamma 2$ subunits of GABA receptor¹³. When bathed in the potassium channels blocker 4-AP, acute slices of FCD from epileptic patients can generate interictal and ictal discharges, but no activity has yet been reported in basal condition³². Blocking GABA_A receptors transformed the ictal activity into regular interictal-like activity (eventually preictal), whereas increasing GABAergic transmission with phenobarbital increased the duration and amplitude of both ictal and interictal events¹². Our study is the first showing spontaneous epileptic activities *in vitro*, stressing the epileptic nature of the studied tissue in presence of eventually large histological defects. In addition, it shows the positive involvement of GABAergic transmission and demonstrates that spontaneous IIDs are triggered rather than controlled by GABA_A signals. Such pharmacological pattern suggests that interictal discharges may be initiated by interneurons, as already shown *in vitro* in human subiculum^{15,24,28}, peritumoral cortex¹⁶, as well as in CA1 *in vivo* using Ca²⁺ imaging network analysis in a mice model of chronic temporal lobe epilepsy⁵⁰. These data may partially explain the pharmacoresistance of FCD. Our results are also in agreement with interictal intracranial recordings of human patients, as intravenous injection of the GABA_A agonist diazepam did not suppress continuous spiking inside the dysplastic cortex⁴².

Third, the selective blockade of NKCC1 by bumetanide stopped IIDs generated in the dysplastic cortex. To our knowledge, this is the first report of the antiepileptic effect of bumetanide in human cortical slices of FCD. NKCC1 drives neuronal chloride influx, supports the depolarizing effect of GABA early in embryogenic life, and is later counterbalanced by KCC2 chloride cotransporter expression that leads to chloride hyperpolarizing currents at GABA_A receptors activation²⁰. NKCC1 expression itself has been shown to be increased in human dysplastic tissues^{18,19,43-45}, especially in type I Ib FCDs^{19,45} and within the dysplastic component^{44,45}. Immunostaining studies showed an increase in NKCC1 immunoreactivity (with the limitation of the specificity of the antibodies) in FCD type I Ib in both neurons (especially those expressing GABA_A receptor subunit $\alpha 1$) and glial cells as compared to control cortex⁴⁵. Our study confirms the functional implication of NKCC1 up-regulation by showing that its blockade controls interictal activities. In contrast, if neuronal somatic KCC2 immunoreactivity was observed in 67% of the cases, their cellular distribution was altered. This was confirmed in both TSC and FCD I Ib post-operative human tissues with an increase of the NKCC1/KCC2 ratio¹⁹. This shift in chloride cotransporter toward embryonic expression may also be worsened by the localization of KCC2 in FCD I Ib, as immunoreactivity was found in the cytoplasm of cytomegalic neurons, but not on the membrane *per se*¹⁹. KCC2 down-regulation seems to occur in normal-looking neurons within

dysplasias¹⁸ suggesting that non-dysplastic components may directly contribute to an impaired synaptic inhibitory function. Such KCC2 dysregulation may differ between FCD subtypes⁴⁶. In FCD Ia and Ib, as well as in IIb type, KCC2 staining is diffuse in the neuropil (resembling normal expression pattern) within the disorganized cortex, while somatic expression is reduced. Moreover, KCC2 staining seems to be increased in the cytoplasm only in type IIb. At a cellular level, KCC2 labelling is mainly intracytoplasmic in giant pyramidal and dysmorphic, while balloon cells do not seem to express at all the co-transporter. Animal models provide non-conclusive data, stressing the need to study human tissues. For example, in the methylxozymethanol acetate rodent model of FCD, KCC2 expression is paradoxically increased⁴⁷, while it is reduced in the neonatal cortex freeze-lesion animal model^{11,48}. Here, we confirm that KCC2 subcellular expression is altered, but whether increased internalization of the receptor or deficient membrane trafficking is responsible remains to be determined.

Translation of these results to patient's pharmacology is premature, as previous clinical studies failed to demonstrate the antiepileptic effect of bumetanide in epileptic newborns with hypoxic encephalopathy despite basic science evidence⁴⁹. However, development of new drugs targeting chloride co-transporters with higher blood brain barrier permeability, longer half-life and transporter specificity to increase their efficiency and decrease the side effects could be an adjunct to classical AEDs in FCD.

CONCLUSION:

In vitro recording of acute cortical slices from human FCD highlights the role of GABAergic transmission in the generation of spontaneous IIDs via a perturbed chloride homeostasis. Such defect, shared with other epilepsies as hippocampal sclerosis and tumor-related epilepsy, suggests that GABAergic/chloride dysfunction may be a common mechanism, which could be considered as an alternative target for the development of new antiepileptic strategies.

Acknowledgements:

We are grateful to the clinical team, namely Dr. Nicole Chemaly for patient recruitment and assessment; Dr. Marie Bourgeois, Dr. Anna Kaminska, Dr. Emma Losito and Dr. Lorella Minotti for EEG and SEEG recordings; Pr. Nathalie Boddaert for imaging; Dr. Pascale Varlet for histology.

We thank ARNP, “Association pour la recherche en neurochirurgie pédiatrique”, and in particular its secretary Mrs. Marie-Hélène Muzy.

We thank College de France, and particularly the Center for Interdisciplinary Research in Biology for hosting our team to perform these experiments, and Dr. Catherine Chiron for her help at INSERM U1129.

We thank the “Fondation des Gueules cassées” for the post-doctoral fellowship funding of Emmanuelle Goubert and the Eranet Neuron III project.

We are grateful to Flora Vasile for her assistance with the manuscript.

Author contributions:

Conception and design of the study: TB, CSR, RN, GH

Acquisition and analysis of the data: TB, ED, CP, EG, BG

Drafting, correcting and reviewing the manuscript: TB, ED, CP, BG, NR, RN, GH

Potential Conflict of Interests: None

REFERENCES

1. Taylor DC, Falconer, Bruton, Corsellis. Focal dysplasia of the cerebral cortex in epilepsy. *J Neurol Neurosurg Psychiatr* 1971;(34):369–387.
2. Blümcke I, Aronica E, Urbach H, et al. A neuropathology-based approach to epilepsy surgery in brain tumors and proposal for a new terminology use for long-term epilepsy-associated brain tumors. *Acta Neuropathol* 2014;128(1):39–54.
3. Blümcke I, Thom M, Aronica E, et al. The clinicopathologic spectrum of focal cortical dysplasias: a consensus classification proposed by an ad hoc Task Force of the ILAE Diagnostic Methods Commission. *Epilepsia* 2011;52(1):158–174.
4. Rowland NC, Englot DJ, Cage TA, et al. A meta-analysis of predictors of seizure freedom in the surgical management of focal cortical dysplasia. *Journal of neurosurgery* 2012;116(5):1035–1041.
5. Hauptman JS, Mathern GW. Surgical treatment of epilepsy associated with cortical dysplasia: 2012 update. *Epilepsia* 2012;53 Suppl 4:98–104.
6. Aubert S, Wendling F, Regis J, et al. Local and remote epileptogenicity in focal cortical dysplasias and neurodevelopmental tumours. *brain* 2009;132(Pt 11):3072–3086.
7. André VM, Flores-Hernández J, Cepeda C, et al. NMDA receptor alterations in neurons from pediatric cortical dysplasia tissue. *Cereb. Cortex* 2004;14(6):634–646.
8. Calcagnotto ME. Dysfunction of Synaptic Inhibition in Epilepsy Associated with Focal Cortical Dysplasia. *Journal of Neuroscience* 2005;25(42):9649–9657.
9. Alonso-Nanclares L, Garbelli R, Sola RG, et al. Microanatomy of the dysplastic neocortex from epileptic patients. *brain* 2005;128(Pt 1):158–173.
10. Medici V, Rossini L, Deleo F, et al. Different parvalbumin and GABA expression in human epileptogenic focal cortical dysplasia. *Epilepsia* 2016;57(7):1109–1119.
11. Fukuda A, Wang T. A perturbation of multimodal GABA functions underlying the formation of focal cortical malformations: assessments by using animal models. *Neuropathology* 2013;33(4):480–486.
12. D'antuono M, Louvel J, Kohling R, et al. GABAA receptor-dependent synchronization leads to ictogenesis in the human dysplastic cortex. *brain* 2004;127(7):1626–1640.
13. André VM, Cepeda C, Vinters HV, et al. Pyramidal cell responses to gamma-aminobutyric acid differ in type I and type II cortical dysplasia. *Journal of Neuroscience Research* 2008;86(14):3151–3162.
14. Cepeda C, Chen JY, Wu JY, et al. Pacemaker GABA synaptic activity may contribute to network synchronization in pediatric cortical dysplasia. *Neurobiol. Dis.* 2014;62:208–217.

15. Huberfeld G, Wittner L, Clemenceau S, et al. Perturbed chloride homeostasis and GABAergic signaling in human temporal lobe epilepsy. *Journal of Neuroscience* 2007;27(37):9866–9873.
16. Pallud J, Le Van Quyen M, Bielle F, et al. Cortical GABAergic excitation contributes to epileptic activities around human glioma. *Sci Transl Med* 2014;6(244):244ra89–244ra89.
17. Shimizu-Okabe C, Okabe A, Kilb W, et al. Changes in the expression of cation-Cl⁻ cotransporters, NKCC1 and KCC2, during cortical malformation induced by neonatal freeze-lesion. *Neuroscience Research* 2007;59(3):288–295.
18. Shimizu-Okabe C, Tanaka M, Matsuda K, et al. KCC2 was downregulated in small neurons localized in epileptogenic human focal cortical dysplasia. *Epilepsy Research* 2011;93(2-3):177–184.
19. Talos DM, Sun H, Kosaras B, et al. Altered inhibition in tuberous sclerosis and type IIb cortical dysplasia. *Ann Neurol.* 2012;71(4):539–551.
20. Cation-chloride cotransporters in neuronal development, plasticity and disease. 2014;15(10):637–654.
21. Najm IM, Sarnat HB, Blümcke I. Review: The international consensus classification of Focal Cortical Dysplasia - a critical update 2018. *Neuropathol. Appl. Neurobiol.* 2018;44(1):18–31.
22. Blümcke I, Mühlebner A. Neuropathological work-up of focal cortical dysplasias using the new ILAE consensus classification system - practical guideline article invited by the Euro-CNS Research Committee. *NP* 2011;30(4):164–177.
23. Dossi E, Blauwblomme T, Nabbout R, et al. Multi-electrode Array Recordings of Human Epileptic Postoperative Cortical Tissue. *JoVE* 2014;(92)
24. Cohen I, Navarro V, Clemenceau S, et al. On the Origin of Interictal Activity in Human Temporal Lobe Epilepsy in Vitro. *Science* 2002;298(5597):1418–1421.
25. Ludwig A, Li H, Saarma M, et al. Developmental up-regulation of KCC2 in the absence of GABAergic and glutamatergic transmission. *Eur. J. Neurosci.* 2003;18(12):3199–3206.
26. Tyzio R, Nardou R, Ferrari DC, et al. Oxytocin-mediated GABA inhibition during delivery attenuates autism pathogenesis in rodent offspring. *Science* 2014;343(6171):675–679.
27. Navarrete M, Alvarado-Rojas C, Le Van Quyen M, Valderrama M. RIPPLELAB: A Comprehensive Application for the Detection, Analysis and Classification of High Frequency Oscillations in Electroencephalographic Signals. *PLoS ONE* 2016;11(6):e0158276.
28. Huberfeld G, Menendez De La Prida L, Pallud J, et al. Glutamatergic pre-ictal discharges emerge at the transition to seizure in human epilepsy. *Nat Neurosci* 2011;14(5):627–634.

29. Dzhala VI, Talos DM, Sdrulla DA, et al. NKCC1 transporter facilitates seizures in the developing brain. *Nat Med* 2005;11(11):1205–1213.
30. Glykys J, Dzhala V, Egawa K, et al. Local impermeant anions establish the neuronal chloride concentration. *Science* 2014;343(6171):670–675.
31. Dossi E, Blauwblomme T, Moulard J, et al. Pannexin-1 channels contribute to seizure generation in human epileptic brain tissue and in a mouse model of epilepsy. *Sci Transl Med* 2018;10(443):eaar3796.
32. Avoli M, Bernasconi A, Mattia D, et al. Epileptiform Discharges in the Human Dysplastic Neocortex: In Vitro Physiology and Pharmacology. *Ann Neurol*. 1999;46(6):816–826.
33. Aronica E, Gorter JA, Jansen GH, et al. Expression and cell distribution of group I and group II metabotropic glutamate receptor subtypes in taylor-type focal cortical dysplasia. *Epilepsia* 2003;44(6):785–795.
34. Finardi A, Colciaghi F, Castana L, et al. Long-duration epilepsy affects cell morphology and glutamatergic synapses in type IIB focal cortical dysplasia. *Acta Neuropathol* 2013;126(2):219–235.
35. Ying Z, Babb TL, Comair YG, et al. Induced expression of NMDAR2 proteins and differential expression of NMDAR1 splice variants in dysplastic neurons of human epileptic neocortex. *J. Neuropathol. Exp. Neurol.* 1998;57(1):47–62.
36. Li S, Yu S, Zhang C, et al. Increased expression of matrix metalloproteinase 9 in cortical lesions from patients with focal cortical dysplasia type IIB and tuberous sclerosis complex. *Brain Research* 2012;1453:46–55.
37. Sukigara S, Dai H, Nabatame S, et al. Expression of astrocyte-related receptors in cortical dysplasia with intractable epilepsy. *J. Neuropathol. Exp. Neurol.* 2014;73(8):798–806.
38. Nakagawa JM, Donkels C, Fauser S, et al. Characterization of focal cortical dysplasia with balloon cells by layer-specific markers: Evidence for differential vulnerability of interneurons. *Epilepsia* 2017;58(4):635–645.
39. Sakakibara T, Sukigara S, Otsuki T, et al. Imbalance of interneuron distribution between neocortex and basal ganglia: Consideration of epileptogenesis of focal cortical dysplasia. *Journal of the Neurological Sciences* 2012;323(1-2):128–133.
40. Barinka F, Druga R, Marusic P, et al. Calretinin immunoreactivity in focal cortical dysplasias and in non-malformed epileptic cortex. *Epilepsy Research* 2010;88(1):76–86.
41. Cepeda C, Andrade VM, Flores-Hernandez J, et al. Pediatric cortical dysplasia: correlations between neuroimaging, electrophysiology and location of cytomegalic neurons and balloon cells and glutamate/GABA synaptic circuits. *Dev. Neurosci.* 2005;27(1):59–76.

42. Chassoux F, Devaux B, Landre E, et al. Stereoelectroencephalography in focal cortical dysplasia: A 3D approach to delineating the dysplastic cortex. *Brain* 2000;123(8):1733–1751.
43. Jansen LA, Peugh LD, Roden WH, Ojemann JG. Impaired maturation of cortical GABAA receptor expression in pediatric epilepsy. *Epilepsia* 2010;51(8):1456–1467.
44. Sen A, Martinian L, Nikolic M, et al. Increased NKCC1 expression in refractory human epilepsy. *Epilepsy Research* 2007;74(2-3):220–227.
45. Aronica E, Boer K, Redeker S, et al. Differential expression patterns of chloride transporters, Na⁺-K⁺-2Cl⁻-cotransporter and K⁺-Cl⁻-cotransporter, in epilepsy-associated malformations of cortical development. *Neuroscience* 2007;145(1):185–196.
46. Munakata M, Watanabe M, Otsuki T, et al. Altered distribution of KCC2 in cortical dysplasia in patients with intractable epilepsy. *Epilepsia* 2007;48(4):837–844.
47. Abbah J, Juliano SL. Altered migratory behavior of interneurons in a model of cortical dysplasia: the influence of elevated GABAA activity. *Cerebral Cortex* 2014;24(9):2297–2308.
48. Wang T, Kumada T, Morishima T, et al. Accumulation of GABAergic neurons, causing a focal ambient GABA gradient, and downregulation of KCC2 are induced during microgyrus formation in a mouse model of polymicrogyria. *Cerebral Cortex* 2014;24(4):1088–1101.
49. Pressler RM, Boylan GB, Marlow N, et al. Bumetanide for the treatment of seizures in newborn babies with hypoxic ischaemic encephalopathy (NEMO): an open-label, dose finding, and feasibility phase 1/2 trial. *The Lancet Neurology* 2015;14(5):469–477.
50. Muldoon , Villette V, Tressard T, et al. GABAergic inhibition shapes interictal dynamics in awake epileptic mice. *Brain* 2015; 138(10), 2875–2890.

FIGURES

Figure 1:

Methodological illustration of the study

A-C: From *in vivo* to *in vitro* electrophysiology: cortex from the ictal onset zone of a patient with FCD Ic generates comparable, yet distinct, interictal and ictal discharges *in vivo* and *in vitro*.

A: SEEG recording from electrode P (parasagittal T1 weighted MRI after electrode implantation) shows spontaneous recurrent pseudo-rhythmic interictal spikes and seizures restricted to an abnormal sulcus in the pre-frontal region.

The label corresponds to the intra-cerebral electrode where the abnormal electrophysiological activities were recorded. The green parallelogram illustrates the orientation of the section used for the cortical sample.

B: Parasagittal T1 weighted MRI after pre-frontal resection.

C: Cortical slice, cut from the seizure ictal onset zone, displays on the pathological sulcus (red circle) spontaneous interictal discharges in physiological ACSF *in vitro*, and recurrent seizures in pro-epileptic conditions.

The electrophysiological traces are superimposed on the corresponding recording electrodes of the MEA.

D: From *in vitro* electrophysiology to histological correlations:

. Left: MEA recording of IIDs from a temporal pole specimen.

. Right: NeuN Immunostaining showing a FCDIIIa, with both radial and tangential dyslamination and clustering of neurons in layers IV.

Figure 2:

Acute cortical slices from FCD patients generate spontaneous IIDs in vitro.

A: Left, example of a cortical slice from a patient with FCD Ic on MEA. Spontaneous interictal activity is observed in 3 distinct cortical clusters (red). Right, histograms of the numbers of active epileptic slices in the study, and boxplots of the percentage of cortical area with spontaneous IIDs.

B: Left, raw LFP recordings from 3 distinct histological subtypes showing spontaneous IIDs, associated with MUA during the spike. Right, zoom of one spike from each histological FCD subtype.

C: Left, scatter plot of the amplitude of IIDs as a function of recording time in 3 different slices from the 3 histological subtypes of FCD showing the heterogeneous pattern in type I and II. Right, box plots of frequency, amplitude and duration of IIDs according to histological subtypes.

Figure 3:

Acute cortical slices from FCD patients generate seizure like activities in pro-epileptic conditions.

A: Example of ictal discharges recorded on 0 Mg²⁺ and 6 mM K⁺ ACSF. After PID cluster (black dots), the seizure starts with an oscillatory pattern (left) or with a low voltage fast activity (LVFA, right), followed by rhythmic bursts.

B: Cortical slice from a patient with FCD IIIb. Spontaneous IIDs (left, red) and ictal discharges (right, red) are partially co-localized, yet ictal discharges propagate in adjacent territories, and some ictal discharges emerge in remote areas.

C: Top, PIDs (black dots) emerge at the transition to seizure with a gradual increase in both amplitude and frequency, and coexist with IIDs (empty circles). Bottom, quantification of IID and PID amplitude, duration and frequency.

D: Left, PIDs display HFOs in both ripple and fast ripple range. Right, quantification of HFO duration and frequency.

Asterisks indicate statistical significance (**, $p < 0.01$)

Figure 4:

GABAergic transmission is involved in the genesis of IIDs.

A: Suppression of IIDs in a patient with FCD IIIb by blocking GABA_A receptors with the antagonist Picrotoxin (100 μ M). The effect is reversed after wash-out in physiological ACSF.

B: Correlation between electrophysiological recordings and histology. Immunostaining of GAD 67 interneurons in zones generating spontaneous IIDs (red frame) versus silent zones (green frame) reveals a significant decrease in the number of interneurons in epileptic areas (histogram). Asterisks indicate statistical significance (*, $p < 0.05$)

Figure 5:

Chloride co-transporters abnormalities support the genesis of IIDs.

A: Suppression of IIDs in a patient with FCD Ic by the NKCC1 blocker bumetanide (8 μ M), reversed after wash-out in physiological ACSF.

B: Immunostaining for KCC2 in an epileptic area (left, red) and in a silent area (right, green) showing decreased membrane expression of KCC2 in epileptic cortex.

C: Fluorescent profile of neural cells for KCC2.

Left: Enlargement of the Gaussian fit values for the membrane expression of KCC2 supports a reduction of KCC2 co-transporters on the cell membrane in areas generating IIDs (red).

Right: the histograms show the significant differences in the relative proportion of KCC2 protein expression localized at the membrane or at the cytoplasm in cortical areas producing IIDs (272 cells) compared to cortical areas devoid of epileptic activity (520 cells).

Asterisks indicate statistical significance (**, $p < 0.001$; ***, $p < 0.0001$)

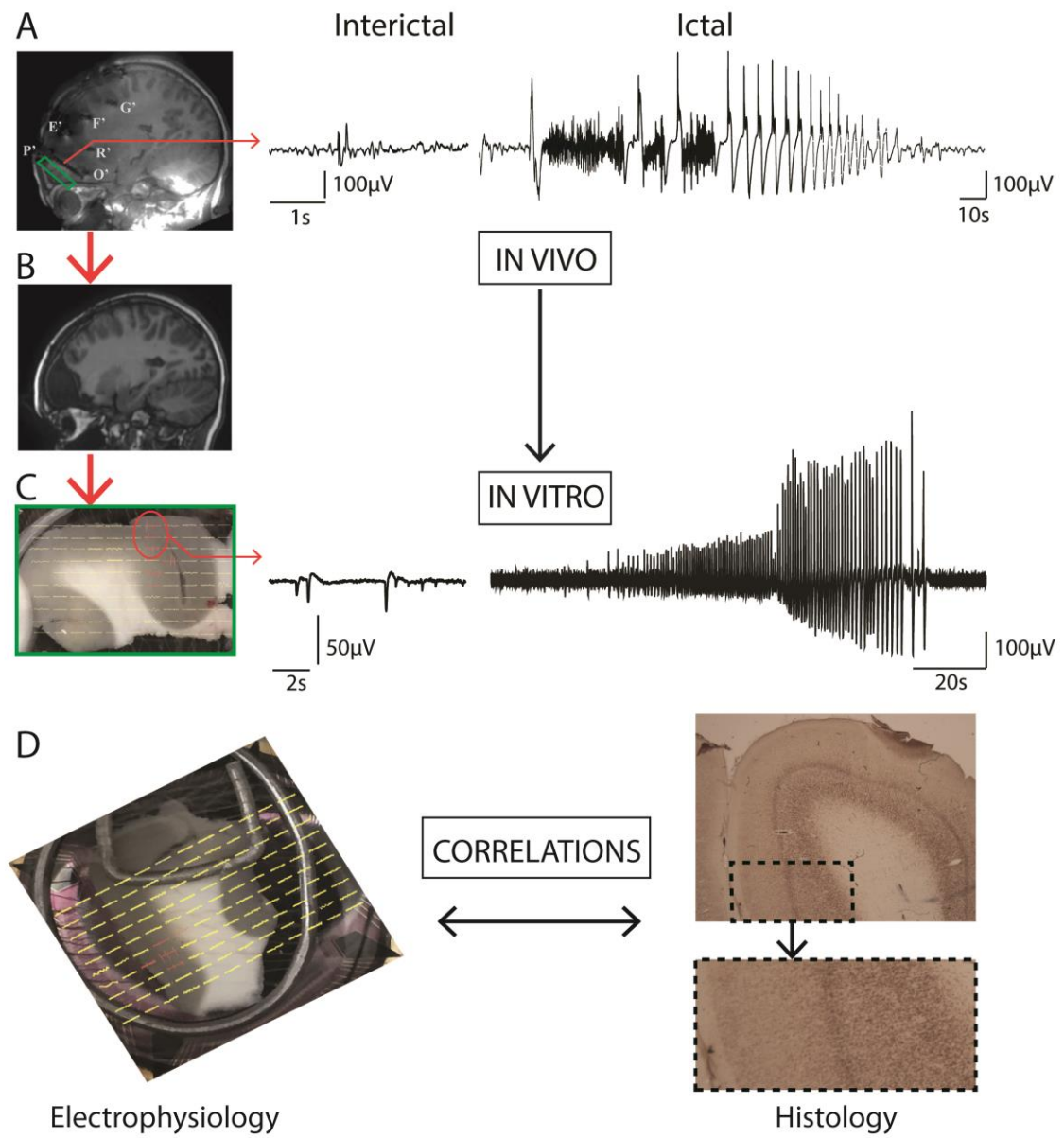
Table

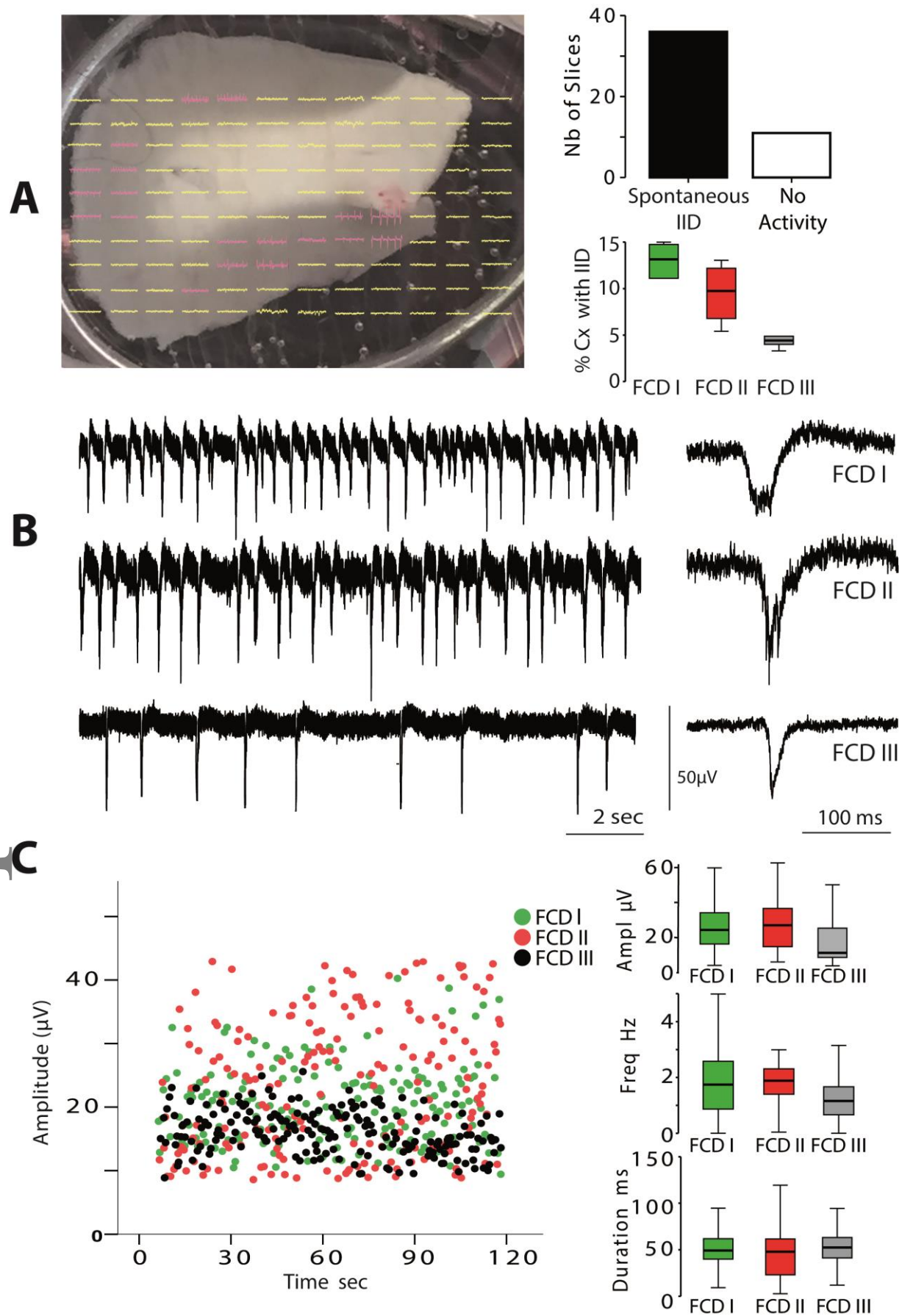
Patients characteristics.

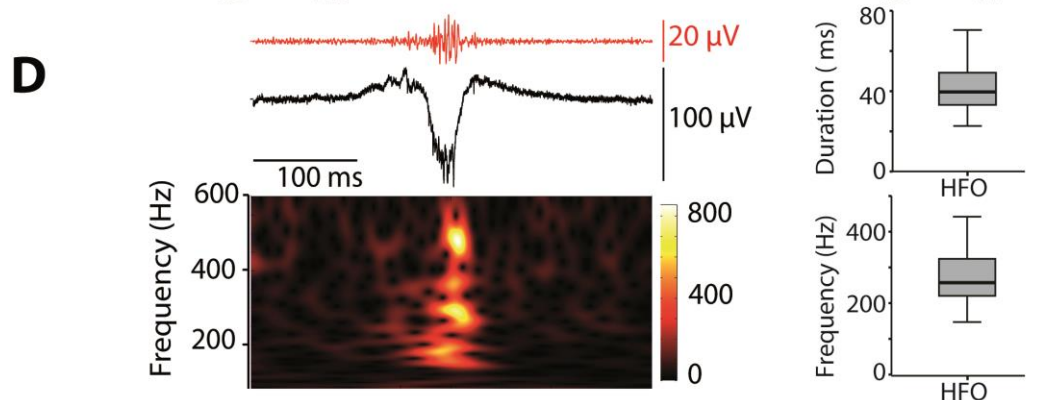
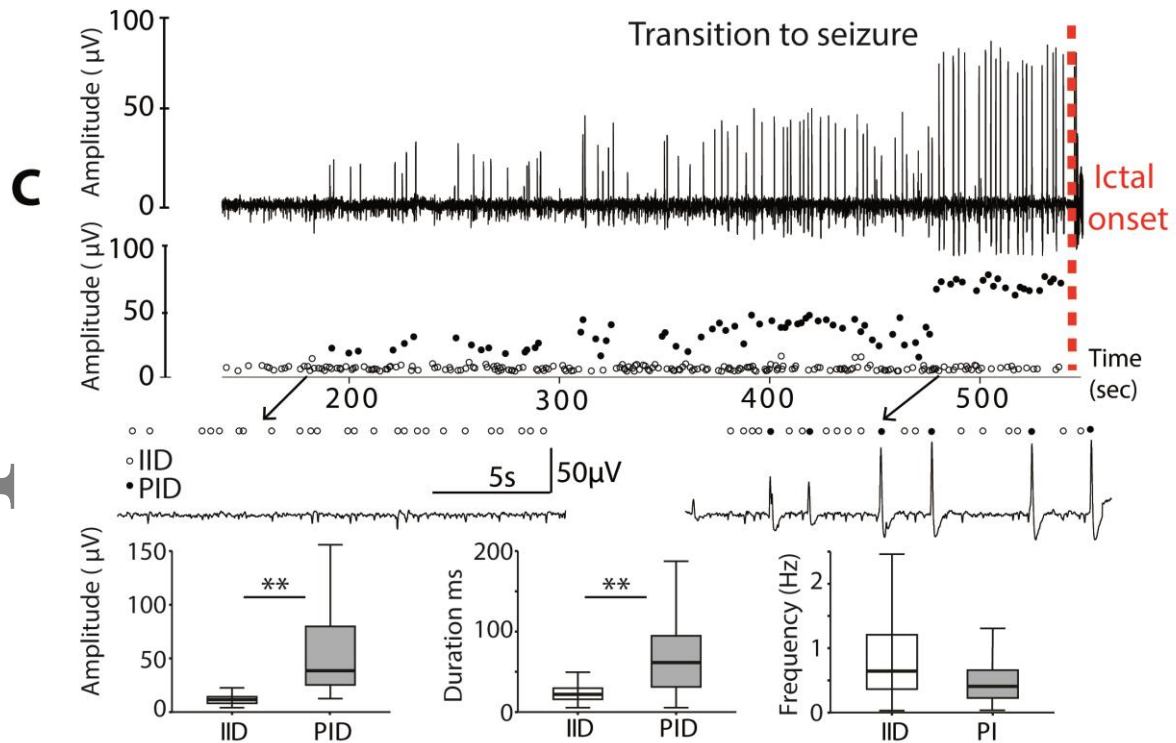
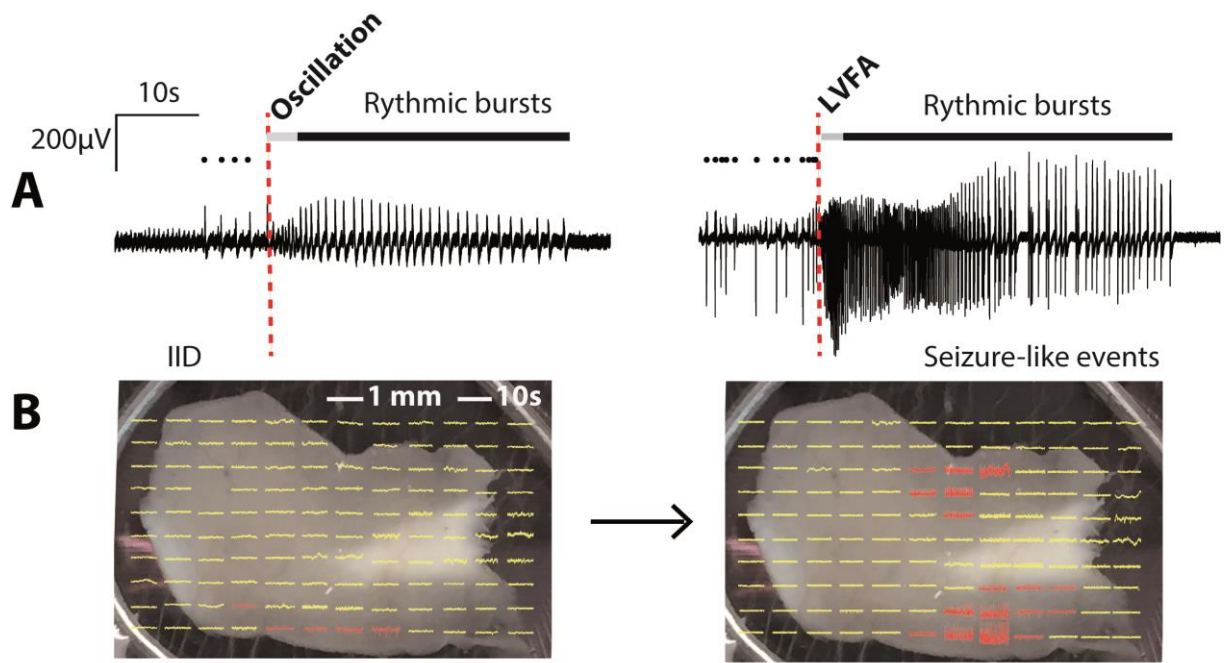
Patient / Sex / Age	Age of 1 st Seizures Sz frequency Seizure semiology	EEG (interictal pattern)	MRI	Number and Name of AEDs at the time of surgery.	Surgery	Localization of Sample	Histology	Number of slices with spontaneous IID
1 / M / 2.8y	6 months >5 Sz/day Epileptic spasms	Spasms posterior quadrant	Right TPO blurring and ASL hypoperfusion	2 Vigabatin / Topiramate	Right posterior quadrant disconnection	Inferior parietal lobule	FCD I b	3/5
2 / M / 5y	18 months 2Sz / day Loss of consciousness Ictal blindness	Rhythmic L occipital spikes	Left occipital lobe cortical thickening G/W matter blurring ASL hypoperfusion	3 Stiripentol / Vigabatin / Topiramate	Left occipital lobectomy	Left occipital pole (V2)	FCD II b	2/3
3 / F / 11y	9y 1Sz/day Gustatory hallucinations / loss of consciousness / Tonic seizures	Rhythmic R frontal spikes and waves	FLAIR hypersignals and ASL hypoperfusion right frontal operculum	3 Carbamazepine / Zonisamide / Clobazam	Right frontal + insular cortectomy after SEEG	Pars opercularis	FCD I c	5 / 6
4 / M / 4.6y	10 months >3 Sz / Day Hypermotor Seizures	Right frontal slow waves	Right frontal lobe hypotrophy and G/W blurring ASL hypoperfusion	3 Lamotrigine / Valproate / Topiramate	Right fronto-insular lobectomy after SEEG	Pars orbitalis	FCD II b + Pial angiomatosis	6/7
5 / F / 9.9y	5 yo 1 Sz / day Focal seizures with impaired awareness	Left temporal spikes and waves	Left temporal lobe G/W blurring and ASL Hypoperfusion FLAIR hypersignals of the	3 Levetiracetam / Lamotrigine / Topiramate	Left anterior temporal lobectomy	Temporal pole	FCD III b + ganglioglioma	4/5

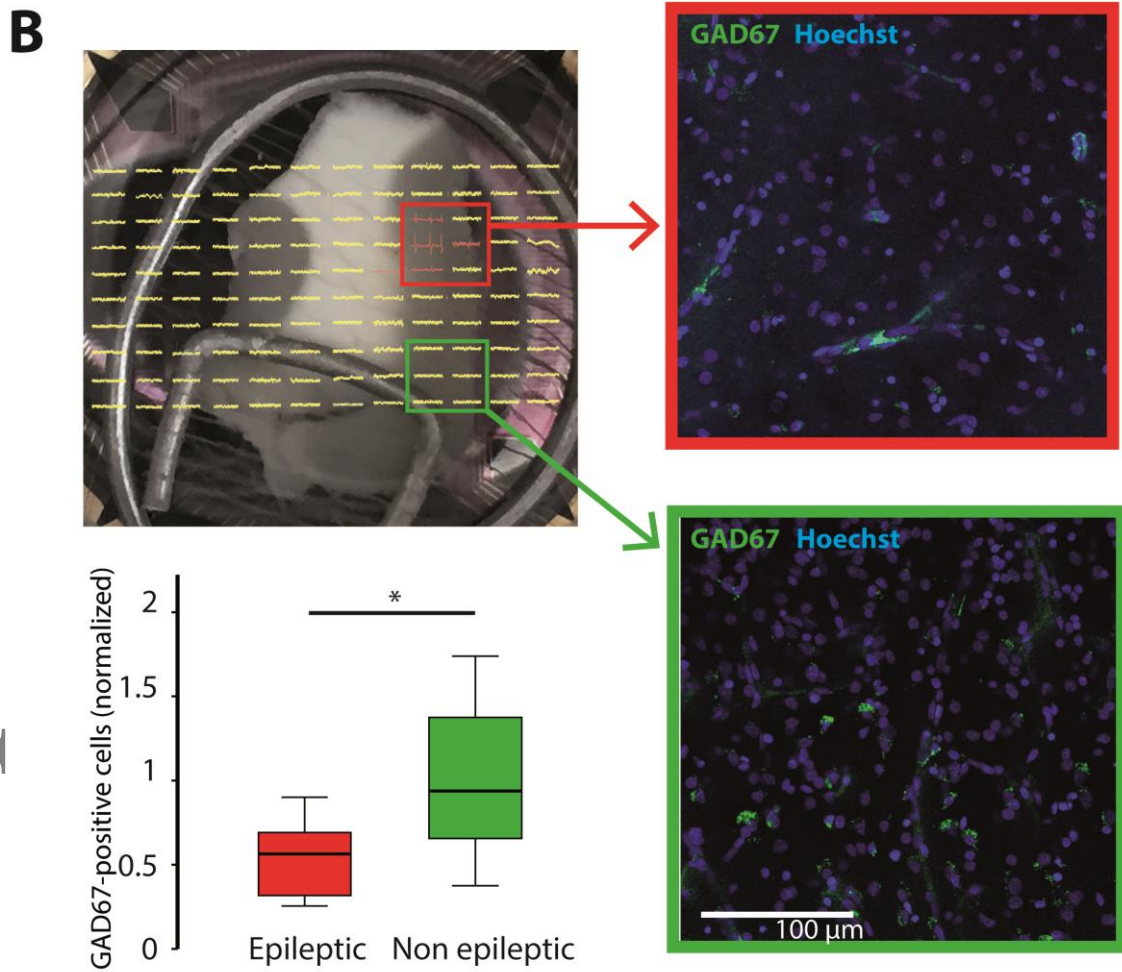
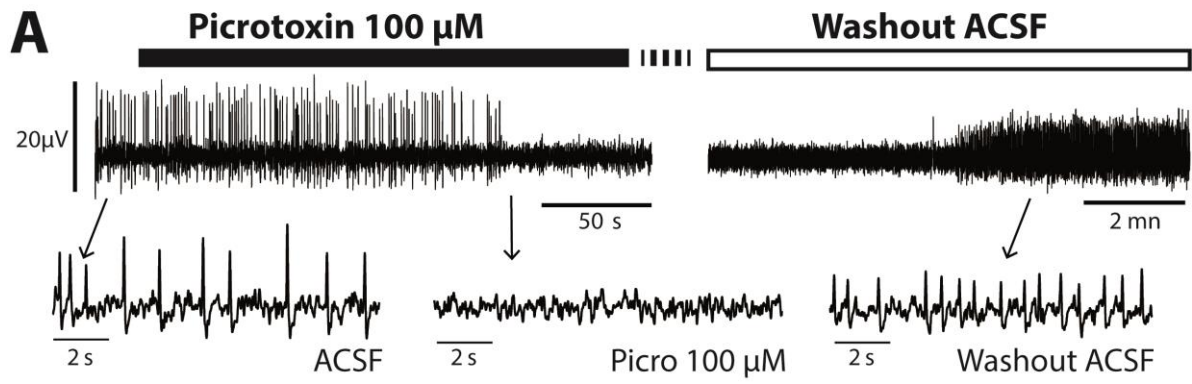
			uncus					
6 / M / 9.4y	7yo 10Sz / day Focal seizures with impaired awareness + motor manifestations	Left fronto temporal slow waves	Left temporal lobe G/W blurring and ASL hypoperfusion	1 Carbamazepine	Left temporo-insular lobectomy after SEEG	Temporal pole	FCD I c + neuronal heterotopia	4/4
7 / F / 7.4y	3yo 1Sz/day Focal seizures with impaired awareness + Head deviation	Rhythmic left spike-wave	Normal morphological MRI F1/F2 sulcal hypoperfusion on ASL	2 Valproate / Lamotrigine	Right frontal pole cortectomy after SEEG	Superior frontal sulcus	FCD I c	3/4
8 / F / 16.9y	3yo >1 Sz /day Focal seizures with impaired awareness	Right temporal slow waves	Right temporal lobe G/W blurring, and ASL hypoperfusion Hippocampal sclerosis	3 Lacosamide / Lamotrigine / Clobazam	Right anterior temporal lobectomy	Temporal pole	FCD III a + Hippocampal sclerosis	4/5
9 / M / 13.1y	1,5yo 1Sz/day Focal seizures with impaired awareness	Right temporal spikes	Right temporal lobe G/W blurring, and ASL hypoperfusion Hippocampal sclerosis	3 Valproate / Carbamazepine / Clobazam	Right anterior temporal lobectomy after SEEG	Temporal pole	FCD III a + Hippocampal sclerosis	1 / 4
10 / M / 8.1y	7yo >3Sz/week Counter-clock wise rotation	Left parietal spikes	Left parietal T2FLAIR Hypersignals ASL Hypoperfusion	2 Carbamazepine / Levetiracetam	Lesionectomy	Left Parietal lobe	FCD IIb	2/2
11 / F / 8 months	3months >1/day Focal seizures	Left temporal slow	Left temporal lobe G/W blurring	2 Valproate / Levetiracetam	Left anterior temporal Lobectomy	Left temporal lobe	FCD Ic	2/2

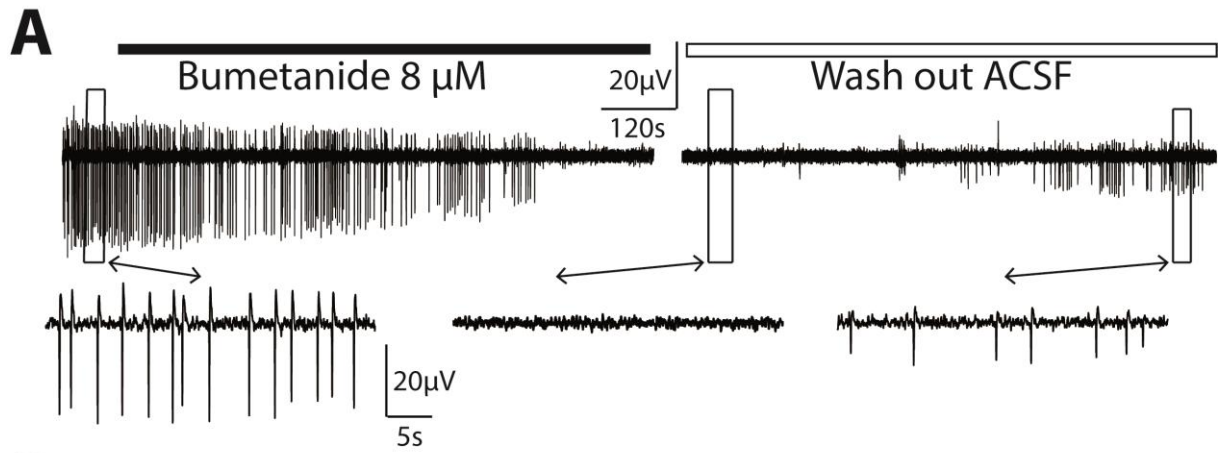
	with impaired awareness	waves and spikes	and ASL hypoperfu sion	tam	y			
--	-------------------------------	------------------------	------------------------------	-----	---	--	--	--



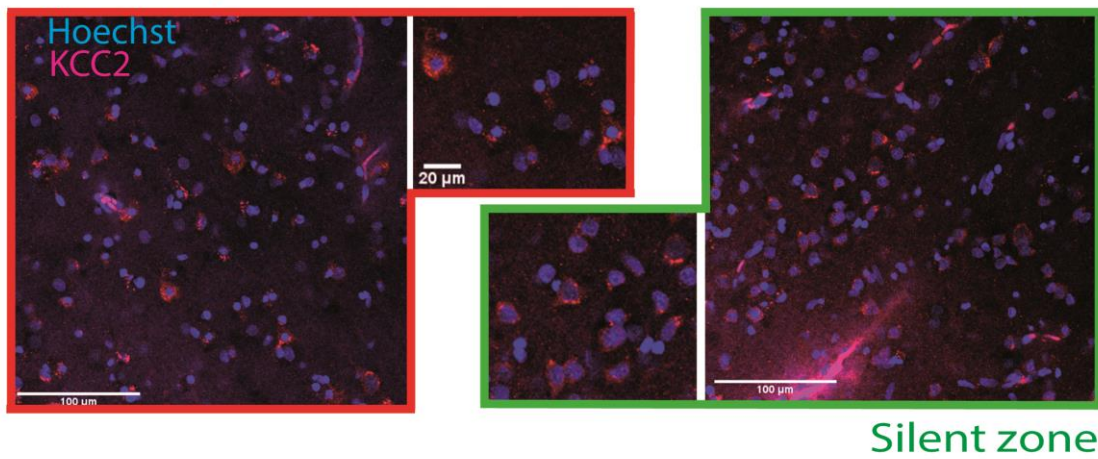








B Zone with spontaneous IID



C

